Reduced Order Model Analysis of Frequency Response of Alternating Current Near Half Natural Frequency Electrostatically Actuated MEMS Cantilevers

Dumitru I. Caruntu[1]
e-mail: caruntud@utpa.edu; caruntud2@asme.org; dcaruntu@yahoo.com

Israel Martinez

Mechanical Engineering Department,
University of Texas-Pan American,
Edinburg, TX 78541

Martin W. Knecht
Engineering Department,
South Texas College,
McAllen, TX 78501

This paper uses the reduced order model (ROM) method to investigate the nonlinear-parametric dynamics of electrostatically actuated microelectromechanical systems (MEMS) cantilever resonators under soft alternating current (AC) voltage of frequency near half natural frequency. This voltage is between the resonator and a ground plate and provides the actuation for the resonator. Fringe effect and damping forces are included. The resonator is modeled as a Euler-Bernoulli cantilever. ROM convergence shows that the five terms model accurately predicts the steady states of the resonator for both small and large amplitudes and the pull-in phenomenon either when frequency is swept up or down. It is found that the MEMS resonator loses stability and undergoes a pull-in phenomenon (1) for amplitudes about 0.5 of the gap and a frequency less than half natural frequency, as the frequency is swept up, and (2) for amplitudes of about 0.87 of the gap and a frequency about half natural frequency, as the frequency is swept down. It also found that there are initial amplitudes and frequencies lower than half natural frequency for which pull-in can occur if the initial amplitude is large enough. Increasing the damping narrows the escape band until no pull-in phenomenon can occur, only large amplitudes of about 0.85 of the gap being reached. If the damping continues to increase the peak amplitude decreases and the resonator experiences a linear dynamics like behavior. Increasing the voltage enlarges the escape band by shifting the sweep up bifurcation frequency to lower values; the amplitudes of losing stability are not affected. Fringe effect affects significantly the behavior of the MEMS resonator. As the cantilever becomes narrower the fringe effect increases. This slightly enlarges the escape band and increases the sweep up bifurcation amplitude. The method of multiple scales (MMS) fails to accurately predict the behavior of the MEMS resonator for any amplitude greater than 0.45 of the gap. Yet, for amplitudes less than 0.45 of the gap MMS predictions match perfectly ROM predictions. [DOI: 10.1115/1.4023164]

1 Introduction

Microelectromechanical systems (MEMS) have received significant attention over the last decades due to their prevalence in a wide range of applications. Small in size, low in weight and energy consumption, these systems are highly durable, making them preferred candidates for a vast array of devices, including accelerometers, relays, RF switches, filters, and sensing applications such as mass flow and chemical sensors, biosensors, immunosensors, or detectors capable of identifying the presence of proteins or DNA strands [1–11]. A MEMS affinity sensor that enables continuous monitoring of glucose for diabetes management, for instance, has been reported in literature [7]. The principle is based on the detection of viscosity changes due to affinity binding between glucose and a biocompatible, glucose-specific polymer. In the case of DNA sensors [11], the principle is based on the detection of the resonance frequency shift induced by the specific DNA immobilization on the resonator. Although various actuation methods for MEMS devices exist, electrostatic actuation is still the most preferred mode of actuation due to its simplicity and efficiency. It provides significant force without requiring the use of special actuation materials and can be controlled through an electric supply which consumes a low amount of energy [12]. In a micro resonator, the electric load is composed of a direct current (DC) polarization voltage and an AC voltage; the beam is deflected by the DC component and then driven to vibrate around its natural frequency by the AC harmonic load [13, 14]. When the combined input voltage exceeds a threshold value, called pull-in voltage, the flexible micro-beam spontaneously deflects and collapses onto the rigid plate, causing the device to fail. This is known as pull-in instability and is a basic instability phenomenon considered in design [15]. Nonlinearity plays a major role at the micron scale; it usually arises from sources, such as squeeze-film damping, electrostatic actuation, large deflections (geometric nonlinearities), and intermolecular forces such as Casimir or van der Waals [16] present at submicron scales. The minimization of damping is an essential requirement in the design of micro resonators, which constitutes a major factor of energy dissipation in such systems [17]. The AC voltage produces an electrostatic force, which is nonlinear and parametric, exciting the MEMS resonator. Understanding the nature of parametric excitations is of general

[1]Corresponding author.

Contributed by the Design Engineering Division of ASME for publication in the JOURNAL OF COMPUTATIONAL AND NONLINEAR DYNAMICS. Manuscript received June 1, 2012; final manuscript received November 29, 2012; published online January 25, 2013. Assoc. Editor: Henryk Flashner.

Copyright © 2013 by ASME

Downloaded 13 Feb 2013 to 129.113.125.56. Redistribution subject to ASME license or copyright; see http://www.asme.org/terms/Terms_Use.cfm

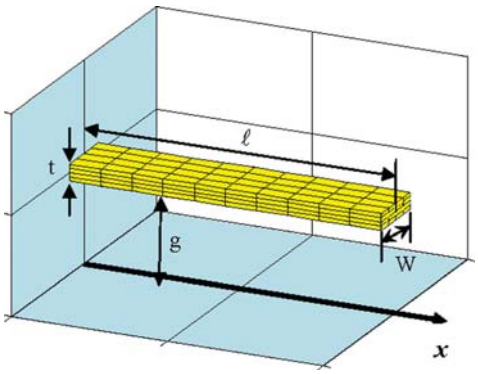

Fig. 1 Uniform MEMS resonator

interest. Parametric excitations can be used to design devices, such as mass sensors, microscopy probes, filters, and resonators. The stability of such systems and the types of nonlinearities that occur are highly sensitive to physical parameters, initial amplitude, and excitation frequency. It is then important to identify bifurcation parameters and bifurcation points in order to design and control systems under parametric excitation. The nonlinear dynamics of clamped-clamped microbeams has been reported in the literature [18, 19]; yet, the fringe effect was not included [18], ROM versus MMS was not investigated, the case of AC soft excitations only has not been considered. Also, nonlinear dynamic response of comb drives [20] has been reported in the literature. Comb drives have been modeled as one-degree-of-freedom systems. Perturbation analysis has been used to find the frequency response. A certain AC voltage has been used to provide the harmonic excitation.

This paper investigates the dynamics of MEMS cantilever (clamped-free) resonator sensors under soft AC voltage of frequency near half natural frequency. This is a nonlinear-parametric excitation. As the electrostatic force is proportional to the square of the voltage, the electrostatic force actuates the cantilever in its primary resonance zone. The ROM method is used to solve the differential equation of motion describing the system. The equation of motion is developed using the Euler-Bernoulli hypothesis of thin beams. The frequency-amplitude response of the MEMS resonator is predicted. Two-term, three-term, four-term, and five-term ROMs are numerically solved using AUTO 07P to predict the amplitude-frequency response curves. A comparison ROM versus MMS [21] is included. To the best of our knowledge, this is the first time when a comparison between ROM and MMS is conducted to investigate MEMS cantilever resonators under soft AC voltage of frequency near the resonator's half natural frequency (resulting in primary resonance) and to include the fringe effect.

2 Differential Equation of Motion

Figure 1 shows an electrostatically actuated MEMS cantilever resonator that consists of a deformable electrode suspended over a ground plate. The boundary value problem of the system is given by [21]

$$\begin{cases} \rho A(x)\dfrac{\partial^2 w(t,x)}{\partial t^2}+\dfrac{\partial^2}{\partial x^2}\left[EI(x)\dfrac{\partial^2 w(t,x)}{\partial x^2}\right]=F_e(t,x)-F_d(t,x) \\ w(t,0)=\dfrac{\partial w}{\partial x}(t,0)=\dfrac{\partial^2 w}{\partial x^2}(t,\ell)=\dfrac{\partial^3 w}{\partial x^3}(t,\ell)=0 \end{cases} \tag{1}$$

where t is time, x is the longitudinal coordinate, ℓ is the beam length, $w=w(x,t)$ is the transverse deflection of the beam, E is the Young's modulus, $I(x)$ is the moment of inertia of the beam's cross section, F_e is the electrostatic force per unit length, and F_d is the damping force per unit length. First order fringing correction [21] is considered such that the electrostatic force per unit length F_e along the beam is

$$F_e(t,x)=\frac{\varepsilon_0 W}{2}\frac{V(t)^2}{[g-w(t,x)]^2}\left\{1+0.65\frac{[g-w(t,x)]}{W}\right\} \tag{2}$$

where $\varepsilon_0=8.854\times10^{-12}\mathrm{C}^2\mathrm{N}^{-1}\mathrm{m}^{-2}$ is the permittivity of free space, W is the beam width, g is the initial gap between the beam and ground electrode, and $V(t)$ is the applied voltage. Damping force per unit length is given by

$$F_d(t,x)=b\frac{\partial w(t,x)}{\partial t} \tag{3}$$

where b is a coefficient of viscous damping per unit length. The viscous damping force is used, and it is assumed that the resonator will operate in a viscous pressure regime [21].

3 Dimensionless Equation

Dimensionless variables are as follows:

$$u=w/g,\quad z=x/\ell,\quad \tau=\frac{1}{\ell^2}\sqrt{\frac{EI_0}{\rho A_0}}\cdot t \tag{4}$$

where $u=u(z,t)$, z and τ are dimensionless beam transverse deflection, dimensionless longitudinal coordinate, and dimensionless time, respectively. Also, A_0 and I_0 are reference cross-section area and reference cross-section moment of inertia. For uniform structures they are the cross-section area and moment of inertia of the cantilever. For nonuniform cantilevers the reference cross-section could be where the cross-section area is maximum [22,23]. The dimensionless boundary value problem results as follows:

$$\begin{cases} A^*(z)\dfrac{\partial^2 u(\tau,z)}{\partial\tau^2}+\dfrac{\partial^2}{\partial z^2}\left(I^*(z)\dfrac{\partial^2 u(\tau,z)}{\partial z^2}\right)=-b^*\dfrac{\partial u(\tau,z)}{\partial\tau}+\dfrac{\delta\cdot V^2(\tau)}{[1-u(\tau,z)]^2}+\dfrac{f\cdot\delta\cdot V^2(\tau)}{[1-u(\tau,z)]} \\ u(\tau,0)=\dfrac{\partial u}{\partial z}(\tau,0)=\dfrac{\partial^2 u}{\partial z^2}(\tau,1)=\dfrac{\partial^3 u}{\partial z^3}(\tau,1)=0 \end{cases} \tag{5}$$

where the dimensionless cross section area A^* and moment of inertia I^* are given by

$$A^*=A/A_0\quad I^*=I/I_0 \tag{6}$$

and A and I are the dimensional quantities. For uniform beams A^* and I^* are equal to 1. The dimensionless voltage $V(\tau)$ in this investigation is considered as follows:

$$V(\tau)=\cos\mathbf{\Omega}^*\tau \tag{7}$$

Downloaded 13 Feb 2013 to 129.113.125.56. Redistribution subject to ASME license or copyright; see http://www.asme.org/terms/Terms_Use.cfm

The dimensionless parameters in Eqs. (5) are given by

$$b^* = \frac{b}{g}\sqrt{\frac{\ell^4}{\rho A_0 E I_0}}, \quad \delta = \frac{\varepsilon_0 W \ell^4}{2g^3 E I_0} V_0^2, \quad f = \frac{0.65g}{W}$$
$$\mathbf{\Omega}^* = \mathbf{\Omega}\ell^2\sqrt{\frac{\rho A_0}{E I_0}} \tag{8}$$

where b^* is the dimensionless damping coefficient, δ is the dimensionless amplitude of the electrostatic excitation force, f is associated with a fringing correction to the electrostatic force, $\mathbf{\Omega}^*$ the dimensionless frequency of excitation, and V_0 the amplitude of the AC voltage.

4 Resonance for $\Omega \approx \omega_k/2$

The frequency of the AC voltage is near half the natural frequency, $\Omega^* \approx \omega_k/2$. The nearness of the excitation frequency can be written as

$$2\mathbf{\Omega}^* = \omega_k + \sigma \tag{9}$$

where σ is a detuning parameter. Substituting Eqs. (7) and (9) into Eq. (5), it results in

$$\frac{\partial^4 u(\tau,z)}{\partial z^4} + \frac{\partial^2 u(\tau,z)}{\partial \tau^2} + b^* \frac{\partial u(\tau,z)}{\partial \tau} = \left\{\frac{\delta}{[1-u(\tau,z)]^2} + \frac{f\cdot\delta}{[1-u(\tau,z)]}\right\}\frac{(1+\cos 2\Omega^*\tau)}{2} \tag{10}$$

One can notice that although the frequency of the AC voltage is near half natural frequency, the frequency of the excitation force is near natural frequency; notice the cosine in Eq. (10). This is nonlinear-parametric primary resonance of the structure.

5 ROM of Uniform MEMS Resonators

A set of nonexplicit ordinary differential equations were developed to model the frequency response of the micro-beam using the ROM. This method, based on the Galerkin procedure, uses the undamped linear mode shapes of the undamped cantilever beam as the basis functions [21, 24]. The solution is assumed as

$$u(z,\tau) = \sum_{i=1}^{N} u_i(\tau)\varphi_i(z) \tag{11}$$

where N is the number of terms, $u_i(\tau)$ are the time dependent coefficients, and $\phi_i(z)$ are the first N linear undamped mode shapes of the uniform cantilever beam given by [21]

$$\phi_k(z) = -\left\{\cos(\sqrt{\omega_k}z) - \cosh(\sqrt{\omega_k}z) + C_k[\sin(\sqrt{\omega_k}z) - \sinh(\sqrt{\omega_k}z)]\right\} \tag{12}$$

where k is any nonzero positive integer, and ω_k are the corresponding natural frequencies. These mode shapes form an orthonormal set. The first five natural frequencies ω_k and coefficients C_k from Eq. (12) are given in Table 1. In order to implement the ROM method the following steps were considered. Equation (10) was multiplied by $[1-u(\tau,z)]^2$ (to eliminate any deflection $u(z,\tau)$ from appearing in the denominator [21]), and then Eq. (11) was substituted into it. Since the following relationships are satisfied by the mode shapes of the cantilever

$$u^{(4)} = \sum_i^N u_i \phi_i^{(4)} = \sum_i^N \omega_i^2 u_i \phi_i \tag{13}$$

the resulting equation is as follows:

$$\sum_i^N \ddot{u}_i\phi_i - 2\sum_{ij}^N \ddot{u}_i u_j \phi_i\phi_j + \sum_{ijk}^N \ddot{u}_i u_j u_k \phi_i\phi_j\phi_k + b^*\sum_i^N \dot{u}_i\phi_i - 2b^*\sum_{ij}^N \dot{u}_i u_j\phi_i\phi_j + b^*\sum_{ijk}^N \dot{u}_i u_j u_k\phi_i\phi_j\phi_k + \sum_i^N \omega_i^2 u_i\phi_i - 2\sum_{ij}^N \omega_i^2 u_i u_j\phi_i\phi_j + \sum_{ijk}^N \omega_i^2 u_i u_j u_k\phi_i\phi_j\phi_k = \delta V^2(\tau) + f\delta V^2(\tau) - f\delta V^2(\tau)\sum_i^N u_i\phi_i \tag{14}$$

Then Eq. (14) was multiplied by mode shape $\phi_n(z)$ and the entire equation was integrated from z = 0 to 1, where $n = 1, 2, ..., N$. Therefore, depending on the number of terms used, this process led to a system of N second order coupled differential equations.

6 Numerical Computation

The resulting system of N second equations has been then transformed into a system of $2N$ first order differential equations

$$\begin{cases} \dot{y}(2k-1) = y(2k) \\ \dot{y}(2k) = \ddot{u}_k \end{cases}, \quad k = 1, 2, \ldots, N \tag{15}$$

by using the following variables:

$$\begin{cases} y(2k-1) = u_k \\ y(2k) = \dot{u}_k \end{cases}, \quad k = 1, 2, \ldots, N \tag{16}$$

The system of differential equations given by Eq. (15) has been then integrated for a microbeam Table 2 with dimensionless parameters given in Table 3. Four cases $N = 2$, $N = 3$, $N = 4$, and $N = 5$ using AUTO 07P, a software package for continuation and bifurcation problems [25] have been considered. Steady-state solutions, both stable and unstable, have been found. In AUTO

Table 1 First five natural frequencies and mode shape coefficients for uniform cantilever

	$k=1$	$k=2$	$k=3$	$k=4$	$k=5$
ω_k	3.51562	22.0336	61.70102	120.91202	199.85929
C_k	−0.734	−1.0185	−0.9992	−1.00003	−1.00000

Table 2 Dimensional system parameters

Parameter	Symbol	Value
Beam width	W	20 μm
Beam length	l	300 μm
Beam thickness	h	2.0 μm
Initial gap distance	g	8.0 μm
Material density	ρ	2330 kg/m^3
Young's Modulus	E	169 GPa
Quality factor	Q	350
Peak ac voltage	V_0	12.5 V

Table 3 Dimensionless system parameters

Damping coefficient	b^*	0.01
Amplitude of excitation	δ	0.10
Fringe correction	F	0.26

Downloaded 13 Feb 2013 to 129.113.125.56. Redistribution subject to ASME license or copyright; see http://www.asme.org/terms/Terms_Use.cfm

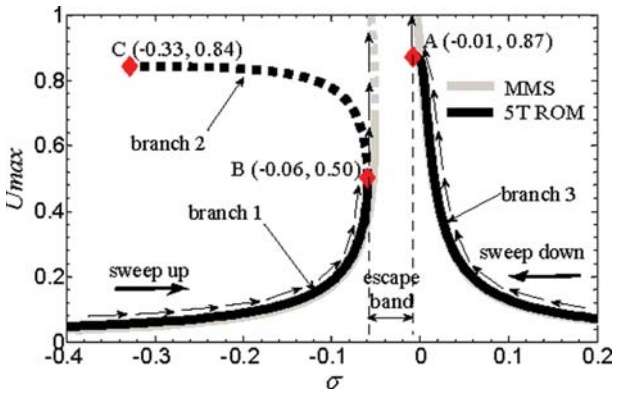

Fig. 2 Amplitude frequency response for AC near half natural frequency using the MMS [21] and a five term ROM (annotated) for dimensionless parameter values $b^* = 0.01$, $\delta = 0.1$, and $f = 0.26$

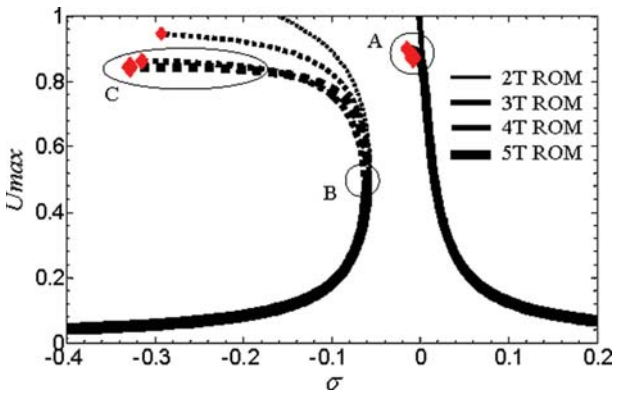

Fig. 3 Amplitude frequency response for AC near half natural frequency using a two, three, four, and five term ROM for dimensionless parameter values $b^* = 0.01$, $\delta = 0.1$, and $f = 0.26$

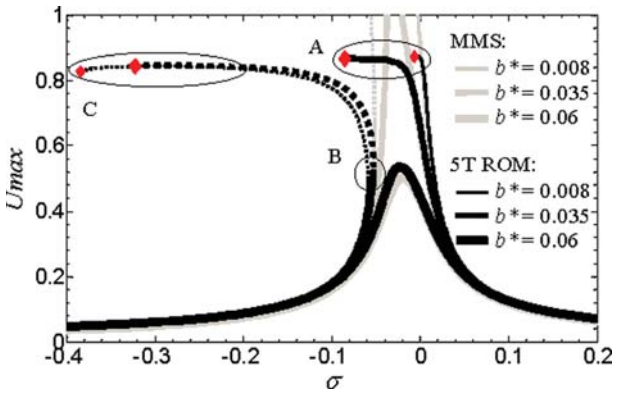

Fig. 4 Amplitude-frequency response showing the influence of the dimensionless damping parameter b^* for dimensionless parameter values $\delta = 0.1$ and $f = 0.26$ using the MMS [21] and a five term ROM

the computation of periodic solutions to a periodically forced system can be done by adding a nonlinear oscillator with the desired periodic forcing as one of the solution components [25]. The frequency-amplitude response of the system for AC near half natural frequency has been investigated using a ROM from the two to five term ROM. The pull-in instability has been predicted.

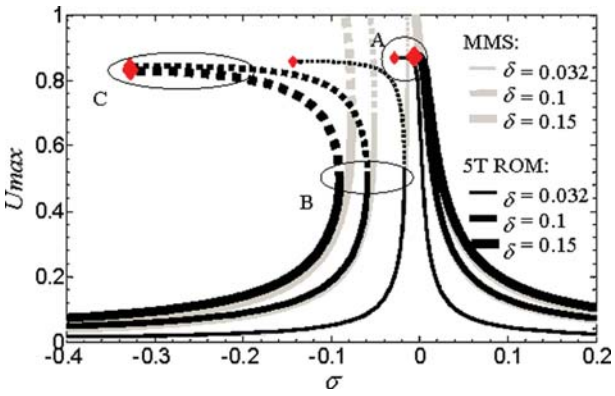

Fig. 5 Amplitude-frequency response showing the influence of the voltage parameter δ for dimensionless parameter values $b^* = 0.01$ and $f = 0.26$ using the MMS [21] and a five term ROM

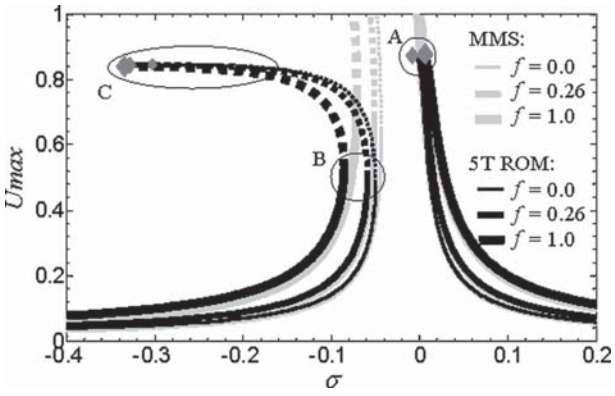

Fig. 6 Amplitude-frequency response showing the influence of the fringe correction f for dimensionless parameter values $b^* = 0.01$ and $\delta = 0.1$ using the MMS [21] and a five term ROM

7 Discussion and Conclusions

This paper investigated the nonlinear dynamics of the MEMS cantilever resonator under soft ac voltage near the resonator's half natural frequency. The resonator is modeled as a Euler-Bernoulli beam. Therefore, no nonlinearities arise from the structure itself. The electrostatic force, including first-order fringe correction, actuating the resonator, induces parametric nonlinear resonances. Parametric coefficients are found in both linear and nonlinear terms within the governing equation. The ROM method based on the Galerkin procedure has been employed. Two term, three term, four term, and five term ROM have been considered in order to show the convergence of the method. AUTO 07P software has been used to numerically solve the resulting system ODEs and generate the amplitude-frequency response. The predictions of the ROM (present work) and MMS [21] have been discussed. ROM was able to accurately capture the behavior of the system where the perturbation method could not [18], i.e., from moderately large deflections up to the pull-in instability limit. Using four or more modes guarantees predicting the pull-in phenomenon [13, 18, 21]. Caruntu and Knecht [21] showed numerical simulations of the pull-in phenomenon. The results of this work are shown in Fig. 2 amplitude-frequency response of the resonator, Fig. 3 ROM convergence, Fig. 4 influence of dimensionless damping, Fig. 5 influence of dimensionless voltage parameter, and Fig. 6 influence of the dimensionless fringe parameter. $U_{\max}$ is the amplitude of the free end of the cantilever.

Figure 2 shows the amplitude-frequency response for five terms (5 T) ROM. This response consists of three branches. Branches 1 and 3 show stable steady-state solutions (solid lines), and branch 2

Downloaded 13 Feb 2013 to 129.113.125.56. Redistribution subject to ASME license or copyright; see http://www.asme.org/terms/Terms_Use.cfm

unstable solutions (dashed lines) [21, 26]. As the frequency is swept up, the amplitude of the resonator increases, along branch 1, until it reaches point B, where a sudden jump to pull-in (contact of the resonator with the ground plate) occurs. As the frequency is swept down, the amplitude of the resonator increases, along branch 3, until it reaches point A, where a sudden jump to pull-in occurs. Branches 1 and 2 together illustrate a saddle-node bifurcation with B the bifurcation point. One can notice the excellent agreement between the MMS and ROM for amplitudes less than 0.5 of the gap. Moreover, on branch 3 the two methods are in agreement up to amplitudes of 0.85 of the gap. One could say that the two methods are in good agreement for amplitudes below points A and B. Yet, MMS fails to accurately predict or predict at all pull-in instability; the amplitude and frequency of point B are overestimated, point A is not predicted. Also MMS fails to predict that pull-in can occur from high initial amplitudes outside the escape band, i.e., MMS fails to predict the unstable branch 2. One can notice that if the initial amplitude is above branch 2, then pull-in occurs. The ROM predicts the amplitude of bifurcation point B to be about 0.5 of the gap, and the amplitude of pull-in instability point A to be about 0.87 of the gap, which is more accurate than Caruntu and Knecht [21] who predicted values of about 0.3 and 0.5, respectively.

Figure 3 illustrates the convergence of the ROM method for the frequency-amplitude response with respect to the number of terms $N = 2, 3, 4, 5$ used in the ROM. As can be noted, changes become less significant with the addition of terms. Numerical simulations conducted in this research demonstrate that four or more terms are required for the ROM to predict pull-in. The convergence shows a very interesting behavior of the system in the higher amplitudes branch 2. As the number of terms in the ROM increases from two to five, the unstable branch of the saddle-node bifurcation converges to branch 2 of Fig. 2. The ROM convergence of the unstable branch has not been predicted by Caruntu and Knecht [21] who limited their study to stable solutions.

Figure 4 shows the effect of the dimensionless damping parameter b^* on the frequency-amplitude response of the resonator using a five term ROM and MMS [21]. For lower damping values, such as $b^* = 0.008$ there is an escape band of frequencies, so the cantilever gets pulled-in from any initial amplitude. As the damping increases the escape band is narrowed until no pull-in phenomenon can occur as the frequency is swept up, only large amplitudes of about 0.85 of the gap being reached; see the case of $b^* = 0.035$. If the damping continues to increase, then the peak amplitude decreases and the resonator experiences a linear dynamics like behavior; see the case of $b^* = 0.06$. As the damping increases the difference in frequency between points A and C becomes smaller and smaller until they coalesce resulting into a linear like behavior of the resonator. From a physical perspective, more air damping translates into a greater amount of energy loss within the MEMS system, meaning the system experiences lower amplitudes for a given voltage. It can be noticed that MMS [21] although predicts the bifurcation point B for $b^* = 0.008$, and it fails to predict B for $b^* = 0.035$. Therefore MMS overestimates the damping related (as the damping increases) transition of the resonator from nonlinear to linear-like behavior.

Figure 5 illustrates the influence of the voltage parameter δ on the amplitude frequency-amplitude response of the MEMS resonator using the five term ROM and MMS [21]. As δ increases the nonlinearities in the system are enhanced: (1) the escape band enlarges, the bifurcation point B being shifted to lower frequencies and the pull-in instability point A to slightly higher frequencies; one can notice that ROM for $\delta = 0.032$ predicts that pull-in cannot occur while the frequency is swept up, only high amplitudes of 0.85 of the gap being possible, (2) the amplitude of the bifurcation point B slightly reduces, (3) the amplitude increases for frequencies outside the escape band, and (4) the area above branch 2 enlarges. MMS, although in good agreement with the ROM at small amplitudes, fails to accurately predict the behavior of the resonator for large amplitudes (1) overestimating the amplitude and frequency of the bifurcation point B; the bifurcation frequency is extremely important if resonators are used as sensors, (2) not predicting the pull-in instability at point A, and (3) not predicting initial high amplitudes (above branch 2) for which pull-in occurs.

Figure 6 shows the influence of the fringe effect correction f on the frequency response of the system using the five term ROM and MMS. Fringing fields emanating from the lateral and top surfaces of the deformable beam need to be accounted for when modeling the electrostatic field. ROM predicts that as the fringe parameter f increases (beam width relative to the gap decreases) branches 1 and 2 are shifted to lower frequencies, and branch 3 to higher frequencies, and therefore 1) the escape band enlarges, the frequency of the bifurcation point B is shifted to lower frequencies, and the frequency of point A to slightly higher frequencies. Also, (2) the amplitude of point B slightly increases, while (3) the amplitude of point A is not affected. For the same frequency, the larger the fringe effect, the larger the amplitude if not pull-in.

One of the possible limitations of this paper is the use of only Palmer's formula for the fringe effect. Other formulas [21], such as Meijs-Fokkema, and Batra-Porfiri-Spinello [27], which are developed for narrow structures, would have allowed for numerical simulations of narrower structures than in the one presented in this work. The geometry of the MEMS resonator in this paper does not necessarily require either Meijs-Fokkema or Batra-Porfiri-Spinello fringe formulas. The Batra-Porfiri-Spinello formula was derived for narrow microbeams with a ratio width/height between 0.5 and 2.0, while in this work this ratio is 10. Also, it has been reported [27] that the Palmer formula gives erroneous values of the capacitance per unit line for narrow microbeams when the ratio width/thickness is between 0.5 and 5, and the ratio gap/thickness is between 0.2 and 2. The corresponding ratios in this work are 10 and 4. Another limitation is that the paper does not include experimental work. This will be the objective of future investigations.

Acknowledgment

This material is based on research sponsored by Air Force Research Laboratory under Agreement No. FA8650-07-2-5061. The U.S. Government is authorized to reproduce and distribute reprints for governmental purposes notwithstanding any copyright notation thereon. The views and conclusions contained herein are those of the authors and should not be interpreted as necessarily representing the official policies or endorsements, either expressed or implied, of Air Force Research Laboratory or the U.S. Government.

References

[1] Badri, A. E., Sinha, J. K., and Albarbar, A., 2010, "A Typical Filter Design to Improve the Measured Signals From MEMS Accelerometer," Measurement, **43**, pp. 1425–1430.
[2] Ozkeskin, F. M., and Gianchandani, Y. B., 2012, "Micromachined Pt-Rh and Stainless Steel Relays for High Power DC Applications," Sens. Actuators, A, **176**, pp. 130–137.
[3] Dumas, N., Trigona, C., Pons, P., Latorre, L., and Nouet, P., 2011, "Design of Smart Drivers For Electrostatic MEMS Switches," Sens. Actuators, A, **167**, pp. 422–432.
[4] Kamali, R., and Binesh, A. R., 2009, "Investigation of Gas Flow in Micro-Filters and Modification of Scaling Law," Int. Commun. Heat Mass Transf., **36**, pp. 763–767.
[5] Tang, M., Cagliani, A., and Davis, Z. J., 2011, "Pulse Mode Readout of MEMS Bulk Disk Resonator Based Mass Sensor," Sens. Actuators A, **168**, pp. 39–45.
[6] Park, K. K., Lee, H., Kupnik, M., Oralkan, O., Ramseyer, J., Lang, H. P., Hegner, M., Gerber, C., and Khuri-Yakub, B. T., 2011, "Capacitive Micromachined Ultrasonic Transducer (CMUT) as a Chemical Sensor for DMMP Detection," Sens. Actuators B, **160**, pp. 1120–1127.
[7] Huang, X., Li, S., Schultz, J. S., Wang, Q., and Lin, Q., 2009, "A MEMS Affinity Glucose Sensor Using Biocompatible Glucose Responsive Polymer," Sens. Actuators B, **140**, pp. 603–609.
[8] Caruntu, D. I., and Knecht, M., 2010, DETC2010-28612, "On MEMS/NEMS Biosensor Sensitivity Near Half Natural Frequency," ASME 2010 Proceedings of International Design Engineering Technical Conferences & Computers and Information in Engineering Conference, DETC2010, Mechanical Vibration and Noise (VIB), August 15-18, The American Society of Mechanical Engineers, Montreal, Quebec, Canada.

Downloaded 13 Feb 2013 to 129.113.125.56. Redistribution subject to ASME license or copyright; see http://www.asme.org/terms/Terms_Use.cfm

[9] Caruntu, D. I., and Knecht, M., 2010, NEMB2010-13238, "Nonlinear parametric resonance for NEMS and MEMS biosensor applications," Proceedings of the ASME 2010 First Global Congress on NanoEngineering for Medicine and Biology NEMB 2010, February 7-10, The American Society of Mechanical Engineers, Houston, TX.
[10] Lu, M., Lee, D., Xue, W., and Cui, T., 2009, "Flexible and Disposable Immunosensors Based on Layer-By-Layer Self-Assembled Carbon Nanotubes and Biomolecules," Sens. Actuators, A, **150**, pp. 280–285.
[11] Adrega, T., Prazeres, D. M. F., Chu, V., and Conde, J. P., 2006, "Thin-Film Silicon MEMS DNA Sensors," J. Non-Cryst. Solids, **352**, pp. 1999–2003.
[12] Stulemeijer, J., Bielen, J. A., Steeneken, P. G., and Bouwe van der Berg, J., 2009, "Numerical Path Following as an Analysis Method for Electrostatic MEMS," J.Microelectromech. Syst., **18**(2), pp. 488–499.
[13] Nayfeh, A. H., Younis, M. I., and Abdel-Rahman, E. M., 2007, "Dynamic Pull-In Phenomenon in MEMS Resonators," Nonlinear Dyn., **48**, pp. 153–163.
[14] Abdel-Rahman, E. M., Nayfeh, A. H., and Younis, M. I., 2003, "Dynamics of an Electrically Actuated Resonant Microsensor," Proceedings of the International Conference on MEMS, NANO and Smart Systems (ICMENS'03), IEEE.
[15] Zand, M. M., Ahmadian, M. T., and Rashidian, B., 2009, "Semi-Analytic Solutions to Nonlinear Vibrations of Microbeams Under Suddenly Applied Voltages," J. Sound Vib., **325**, pp. 382–396.
[16] Ramezani, A., Alasty, A., and Akbari, J., 2007, "Closed-Form Solutions of the Pull-In Instability in Nano-Cantilevers Under Electrostatic and Intermolecular Surface Forces," Int. J. Solids Struct., **44**, pp. 4925–4941.
[17] Zamanian, M., and Khadem, S. E., 2010, "Analysis of Thermoelastic Damping in Microresonators by Considering the Stretching Effect," Int. J. Mech. Sci., **52**, pp. 1366–1375.
[18] Younis, M. I., Abdel-Rahman, E. M., and Nayfeh, A. H., 2003, "A Reduced-Order Model for Electrically Actuated Microbeam-Based MEMS," J. Microelectromech. Syst., **12**(5), pp. 672–680.
[19] Moghimi Zand, M., Ahmadian, M. T., and Rashidian, B., 2009, "Semi-analytic Solutions to Nonlinear Vibrations of Microbeams under Suddenly Applied Voltages," J. Sound Vib., **325**, pp. 382–396.
[20] Rhoads, J. F., Shaw, S. W., Turner, K. L., Moehlis, J., DeMartini, B. E., and Zhang, W., 2006, "Generalized Parametric Resonance in Electrostatically Actuated Microelectromechanical Oscillators," J. Sound Vib., **296**, pp. 797–829.
[21] Caruntu, D. I., and Knecht, M., 2011, "On Nonlinear Response Near Half Natural Frequency of Electrostatically Actuated Microresonators," Int. J. Struct. Stab. Dyn., **11**(4), pp. 641–672.
[22] Caruntu, D. I., 2007, "Classical Jacobi Polynomials, Closed-Form Solutions For Transverse Vibrations," J. Sound Vib., **306**(3–5), pp. 467–494.
[23] Caruntu, D. I., 2009, "Dynamic Modal Characteristics of Transverse Vibrations of Cantilevers of Parabolic Thickness," Mech. Res. Commun. **33**(3), pp. 391–404.
[24] Caruntu, D. I., and Solis Silva, J. C., 2011, IMECE2011-64854, "Reduced Order Model of MEMS Sensors Near Natural Frequency", ASME Proceedings of International Mechanical Engineering Congress and Exposition 2011, November 11–17, Denver, CO, © The American Society of Mechanical Engineers.
[25] Doedel, E. J., and Oldeman, B. E., 2009, "AUTO-07P: Continuation and Bifurcation Software For Ordinary Differential Equations," Concordia University, Montréal, Canada.
[26] Caruntu, D. I., and Knecht, M., 2009, IMECE2009-10663, "Parametric Response of Capacitive Sensors Near Half of Natural Frequency," ASME Proceedings of International Mechanical Engineering Congress and Exposition 2009, November 13-19, The American Society of Mechanical Engineers, Lake Buena Vista, FL.
[27] Batra, R. C., Porfiri, M., and Spinello, D., 2006, "Electromechanical Model of Electrically Actuated Narrow Beams," J. Microelectromech. Syst., **15**, pp. 1175–1189.

Downloaded 13 Feb 2013 to 129.113.125.56. Redistribution subject to ASME license or copyright; see http://www.asme.org/terms/Terms_Use.cfm